Available online at www.sciencedirect.com
ScienceDirect
Journal of Applied Geophysics 61 (2007) 279–291
JOURNAL OF APPLIED GEOPHYSICS
www.elsevier.com/locate/jappgeo

Application of a library based method to time domain electromagnetic data for the identification of unexploded ordnance

Leonard R. Pasion [a,*], Stephen D. Billings [b], Douglas W. Oldenburg [a], Sean E. Walker [b]

[a] UBC Geophysical Inversion Facility, Department of Earth and Ocean Sciences, 6339, Stores Road, University of British Columbia, Vancouver, BC, Canada V6T 1Z4
[b] Sky Research Inc., Suite 112A, 2386 East Mall, Vancouver, BC, Canada V6T 1Z3

Received 17 November 2005; accepted 30 May 2006

Abstract

A simple library based algorithm for the identification of unexploded ordnance is tested on time domain electromagnetic data. A library of polarization tensors is generated from data acquired on a test stand over a collection of different UXO. The objective of the algorithm is to determine which target of the library is most likely to have produced an observed data anomaly. For each target in our library a non-linear inverse problem is solved for the position and orientation that minimizes the least-squares difference between the observed data anomaly and the data predicted from each target. This technique avoids direct inversion for polarization tensor, making it feasible for cases where sensor data quality may not be sufficient to support confident estimation of model parameters. For cases where the background soil response is significant, we also invert for the t^{-1} decay characteristic of viscous remnant magnetic soil. We present results of preliminary tests of the library technique to Geonics EM63 time domain electromagnetic data collected on a test plot seeded with UXO. These tests demonstrate an excellent ability to accurately identify isolated targets. Misidentification of single targets occur when data anomalies have low signal to noise ratios or when targets within the library have similar polarization tensors.
© 2006 Elsevier B.V. All rights reserved.

Keywords: UXO; Time domain electromagnetics

1. Introduction

Electromagnetic induction surveys are a standard geophysical technique used in UXO remediation projects. Electromagnetic detection of a buried target is accomplished by illuminating the subsurface with a time varying primary field. If the buried target is conductive, eddy currents will be induced in the target, and subsequently decay. These currents produce a secondary magnetic field which is then sensed by a receiver coil at the surface. Electromagnetic induction surveys have proven to be successful in detecting UXO in recent remediation projects and technology demonstrations. The goal of geophysical data interpretation is not simply to detect UXO, but rather to discriminate anomalies originating from intact UXO from anomalies due to exploded ordnance and other metallic scrap.

Several data processing techniques for geophysical survey data have been developed for discriminating

* Corresponding author.
E-mail address: lpasion@eos.ubc.ca (L.R. Pasion).

0926-9851/$ - see front matter © 2006 Elsevier B.V. All rights reserved.
doi:10.1016/j.jappgeo.2006.05.006

between UXO and non-UXO items. These techniques rely on recovering the parameters of a physics-based model that can reproduce the observed anomaly (for example Bell et al., 2001a; Grimm, 2003; Zhang et al., 2003; Pasion and Oldenburg, 2001). The dipolar nature of the electromagnetic responses of compact metallic objects measured with sensor/target geometries typical for UXO surveys (Casey and Baertlein, 1999; Grimm et al., 1997) has led to a number of techniques for estimating the elements of the magnetic polarization tensor that define the induced dipole strength. The magnetic polarization tensor's components are functions of the size, shape, and material properties of the buried target of interest and therefore provide a model vector from which the target characteristics can be inferred. Target identification is then achieved by using the recovered model parameters as part of feature vectors that are input into statistical classification algorithms (for example Billings, 2004; Collins et al., 2001; Beran, 2005; Grimm, 2003).

The success of dipole model based discrimination algorithms depends on the accuracy with which the axial and transverse components of the polarization tensor can be estimated. In many cases, however, the data are not of sufficient quality to allow the polarization parameters to be recovered through an inversion (Pasion et al., 2004; Bell, 2005). Poor data quality, due to a low signal to noise ratio or survey design (for example, poor spatial coverage and inadequate illumination of both axial and transverse excitations), make the use of parameter estimation difficult. In such cases, a-priori information can be introduced when searching model, or feature, space. Examples of a-priori information include target location estimates from processing previously acquired data sets (for example, magnetics (Zhang et al., 2003; Pasion et al., 2003) or ground penetrating radar (Shamatava et al., 2004)), and restricting the model type to be rod-like targets. Using a-priori information improves the accuracy of recovered model parameters.

A further restriction in model space would be to assign higher probabilities to encountering different targets. A simple implementation of this concept is to develop a list of candidate UXO likely to be encountered during a survey, and then to determine, for each member of the library, the likelihood of generating the anomaly. Norton et al. (2001) and Riggs et al. (2001) use a single frequency spectrum collected at one location to determine the optimal target from a library. Tantum and Collins (2001) process a single time decay sounding with a library of known exponential decay parameters. The response measured at a single location is a linear function of the dipole polarization tensor, and the technique is fast. However, it does not utilize the additional information provided by data acquired at a number of points spatially distributed on the surface above the target.

In this paper we apply a simple library based technique to time domain electromagnetic data for the identification of UXO. High quality test stand data acquired over a collection of UXO are inverted for polarization tensors. The polarization tensors are functions of the target only and, therefore, are used to characterize each member of the library. A simple matching scheme has been used to estimate the target type from measured TEM anomalies from this library of polarization tensors. For each polarization tensor within the library, a template is generated. The template is defined as the data predicted by the polarization tensor that best fits the observed data. Generating this template requires solving a non-linear inverse problem for the orientation and location of a target. Each of the data templates is then compared to the observed data. To determine if the anomaly is likely generated by one of the targets we can either find the template with the minimum error (for example, least squares) or the maximum correlation to the observed data. By not inverting for model parameters directly, we avoid trade-offs between polarization tensor values and orientation and position that can occur. This method is not meant to replace parametric inversion, but rather provides an additional analysis tool when working with data that does not support inverting for model parameters directly.

2. Methods

2.1. Dipole modeling of TEM data

The electromagnetic response of the target will be primarily dipolar for the target/sensor geometries of UXO surveys. The induced dipole is

$$m(t) = \frac{V}{\mu_0} A^{\mathrm{T}} F(t) A \cdot b^{\mathrm{P}} \tag{1}$$

where V is the volume of the object, A is the Euler rotation tensor, b^{P} is the primary field generated by the sensor transmitter loop, and F is the magnetic polarization tensor. The magnetic polarization tensor is dimensionless. The target's shape, size, and material properties (i.e. conductivity and magnetic susceptibility) are contained in F. The polarization tensor $F(t)$ has the form

$$F(t) = \begin{bmatrix} L_3(t) & 0 & 0 \\ 0 & L_2(t) & 0 \\ 0 & 0 & L_1(t) \end{bmatrix} \tag{2}$$

where $L_2(t)=L_3(t)$ for axi-symmetric targets. In a typical survey TEM soundings will be acquired at a number of different locations by moving the transmitter and receiver along the surface, thereby illuminating the target at a number of different angles. This, in turn, causes different components of the polarization tensor to be preferentially excited.

Analytic expressions for the time domain response $L_i(t)$ are restricted to a metallic sphere, and even an expression for a permeable and conducting non-spherical axi-symmetric body is not available. In general, the time decay for a conductive body of arbitrary size and shape in an insulating medium illuminated by a step-off primary field can be represented by an infinite sum of exponentials (Kaufman, 1994). The infinite sum is still needed even for an axi-symmetric target (for example Carin et al., 2001). While it is possible to truncate these representations and model the TEM response with a number of exponents (Snyder et al., 1999), the inverse problem to determine the weights and time constants is potentially difficult (Istratov and Vyvenko, 1999). Therefore, our approach is to parameterize $L(t)$ with a simple empirical function defined by a minimum number of parameters that seems to have enough flexibility to replicate all the features of the TEM decay.

A sphere is a subset of the class of axi-symmetric targets, and its time decay is determined by the sum of exponentials. Therefore, the form for $L(t)$ should, at least, be able to duplicate the time decay features observed for the sphere. Fig. 1 shows the time derivative response for both a magnetically permeable ($\mu_r=150$) and nonpermeable ($\mu_r=1$) sphere with a radius of 2.5 cm and a conductivity of 3.54×106 S/m in a uniform step-off magnetic field. We focus on the response and its parameterization $\partial L(t)/\partial t$, since the data we consider in this paper are from induction loop sensors.

The time decay of a sphere can be divided into early, intermediate, and late time stages. At early time both magnetically permeable and non-permeable spheres have a characteristic power law decay of $t^{-1/2}$. The intermediate time stage has a characteristic decay of $t^{-3/2}$ and is only evident in the response of permeable spheres. At late time the sphere response is an exponential decay $\exp(-t/\tau_o)$, where τ_o is the fundamental time constant:

$$\tau_o = \frac{\sigma\mu_r\mu_o a^2}{q_1^2} \tag{3}$$

where q_1 is determined by solving the transcendental equation

$$\tan q_s = \frac{(\mu_r-1)q_s}{q_s^2+(\mu_r-1)}. \tag{4}$$

(Kaufman, 1994). The fundamental time constant for a non-permeable sphere is $\tau_o(\mu_r=1)=\sigma\mu_o a^2/\pi^2$. The value of q_1 approaches 4.4934 as μ_r approaches infinity. Therefore, for highly permeable spheres $\tau_o(\mu_r=\infty)=\sigma\mu_r\mu_o a^2/(4.4934)^2$. The dashed lines in Fig. 1 represents fits to the function $\exp(-t/\tau_o)$, where $\tau_o=0.29$ ms for the non-permeable sphere and $\tau_o=20.6$ ms for the permeable sphere.The transition from the $t^{-1/2}$ early time decay to the $t^{-3/2}$ intermediate decay is defined by:

$$\tau_1 = \tau_o\left(\frac{q_1}{\mu_r}\right)^2 \tag{5}$$

(Bell et al., 2001b; Smith et al., 2004). Weichman (2004) refers to τ_1 as the *magnetic crossover time*. He derives the expressions for τ_o and τ_1 for general compact permeable

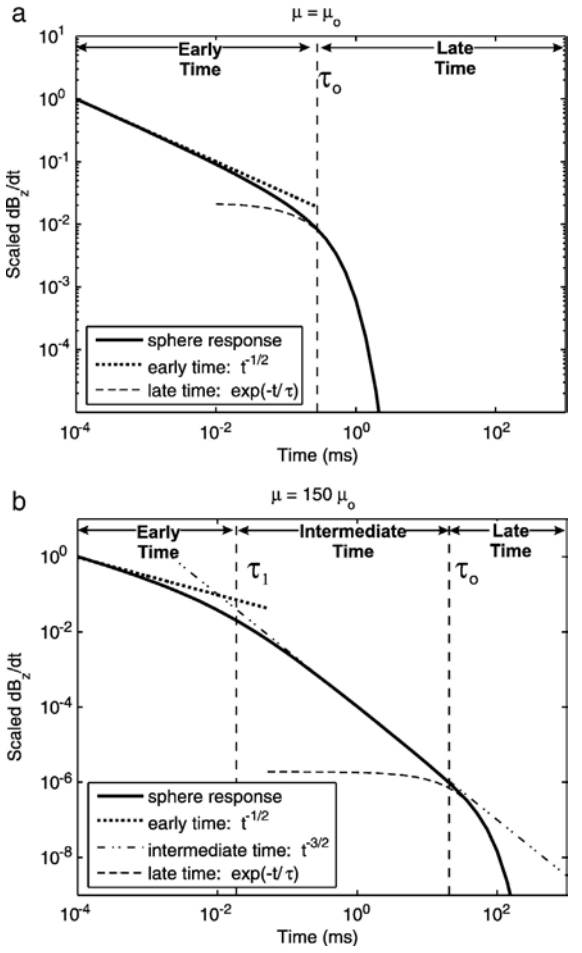


Fig. 1. (a) Non-permeable sphere, (b) permeable sphere. The time decay behavior of a sphere in a uniform field. The sphere has a radius of 2.5 cm and conductivity of 3.54×10^6 S/m. The sphere in (a) has a relative permeability $\mu_o=1$ and the sphere in (b) has a relative permeability of $\mu_o=150$. Both data plots are normalized such that the response is unity at $t=0.0001$ ms.

and conductive targets. Steel targets will typically have $\mu_r > 100$ and, therefore have magnetic crossover times that are approximately four orders of magnitude less than their fundamental time constant, i.e. $\tau_1/\tau_o = O(10^{-4})$. For the example of Fig. 1(b), the magnetic crossover time of $\tau_1 = 0.0185$ is indicated with a vertical dashed line.

The three stages observed for the sphere response was been observed in measured polarization decays of UXO targets (Pasion, 1999). The decays were recorded from 0.01 ms to 100 ms with a Geonics PROTEM47 time domain sensor using a 40 m square transmitter loop. We observed that when there was a transition from early to intermediate time stages, the magnetic crossover time τ_1 was less than 0.1 ms. The fundamental time constants τ_o were less than 100 ms, and had a median of approximately 10 ms. In this paper we analyze data from a Geonics EM63 time domain sensor. The Geonics EM63 measures the time domain response from 0.18 ms to 25 ms, and therefore we only have to model a power law decay followed by the late stage exponential decay.

Several parametric forms for $L(t)$ have been considered (Bell et al., 2001b; Smith et al., 2004; Pasion, 1999). In this paper we use a parameterization suggested by J.D. McNeill (personal communication)

$$\frac{\partial L_i}{\partial t} = k_i t^{-\beta_i} \exp(-t/\tau_i) \tag{6}$$

where k_i controls the magnitude of the polarization, β_i defines the power law decay and τ_i is the fundamental time constant. Eq. (6) is the simplest parameterization that can model a power law decay followed by an exponential. Although it is straightforward to use a parameterization that models the transition from the early time stage to the intermediate time stage, we choose the McNeill parameterization because the Geonics EM63 data will be unable to resolve parameters related to the magnetic crossover time. Pasion and Oldenburg (2001) successfully modeled Geonics EM63 data using Eq. (6).

2.2. Inversion of TEM data

For a data set d^{obs}, the solution to the inverse problem is the combination of the information known about the model parameters m prior to the experiment and the ability of our physical forward modeling $F[m]$ to reproduce the sensor data. This philosophy is reflected by Bayes theorem:

$$p(m|d^{\text{obs}}) = \frac{p(m)p(d^{\text{obs}}|m)}{p(d^{\text{obs}})} \tag{7}$$

where $p(m)$ is the probability distribution representing prior information, $p(d^{\text{obs}})$ is the marginal probability density of the experimental data, and $p(d^{\text{obs}}|m)$ is the conditional probability density of the experimental data which describes the ability of the model to reproduce the experimental data. The a-posteriori conditional probability density $p(m|d^{\text{obs}})$ is the probability density we ascribe to m after collecting the data. The a-posteriori conditional probability density encapsulates all the information we have on the model parameters, given the experimental data, and the model that maximizes it is usually regarded as the solution to the inverse problem. We estimate a value of m that maximizes the log of the a-posteriori conditional probability density

$$m^* = \max_m \{\log(p(m|d^{\text{obs}}))\} \tag{8}$$

Therefore the solution to the inverse problem can be cast as an optimization problem. When data sets are inverted co-operatively, information derived previously are introduced into the inversion through the prior $p(m)$. Commonly utilized priors include Gaussian priors and uniform priors (i.e. a constant pdf for a parameter between two limits, and zero probability outside these limits). The inverse problem solution that utilizes these priors is to

$$\begin{aligned} &\text{minimize } \phi(m) \\ &= \sum_j \frac{1}{2\sigma_j^2}(m_j - \bar{m}_j)^2 \\ &\quad + \frac{1}{2}||V_d^{-1/2}(d^{\text{obs}} - F[m])||^2 \text{ subject to } m_i^L \le m_i \le m_i^U \end{aligned} \tag{9}$$

where j represents the index of parameters whose Gaussian pdf's are known, V_d is the co-variance matrix of the data, and i represents model parameters which have upper and lower bounds. If we assume no prior information and we assume Gaussian statistics for the conditional probability density of the experimental data, then the inverse problem is equivalent to minimizing the data misfit:

$$\text{minimize } \phi(m) = \frac{1}{2}||V_d^{-1/2}(d^{\text{obs}} - F[m])||^2 \tag{10}$$

where V_d is the co-variance matrix of the data.

2.3. A simple library method for identifying UXO

The objective of our template matching analysis is to determine, from a list of M targets, the target that is most

Table 1
Description of UXO in our target library

Type	Description	Length (cm)	Diameter (cm)	Weight (lb)
ATC 20 mm	20 mm M55	7.5	2.0	0.25
ATC 40 mm	40 mm M385	8.0	4.0	0.55
ATC M42	Submunition	6.2	4.0	0.35
ATC BLU-26	Submunition	6.6	6.6	0.95
ATC BDU-28	Submunition	9.7	6.7	1.70
ATC MK118	MK118 Rockeye	34.4	5.0	1.35
ATC 60 mm	60 mm M49A3	24.3	6.0	2.90
ATC 81 mm	81 mm M374	48.0	8.1	8.75
ATC M230	2.75″ Rockeye	76.1	7.5	18.20
ATC 105 mm	M456 heat rd	64.0	10.5	19.65
ATC 155 mm	155 mm M483A1	87.0	15.5	56.45
MTANG 76 mm	Artillery	22.0	7.6	13.50
MTANG 81 mm	Mortar	27.3	8.1	6.00
MTANG 96 mm	Artillery	25.0	9.0	22.50

likely to have generated the observed data d^{obs}. Each target in our list is characterized by its polarization tensor, which we represent by the vector p_i. For each polarization tensor in our library, we determine the location r_i and orientation, represented by angles θ_i and ϕ_i, at which we can best fit the observed data d^{obs} by obtaining the maximum likelihood solution. The data predicted by this recovered model, $d_i^{\text{pred}}=F[r_i, \theta_i, \phi_i, p_i]=F[m_i]$, is referred to as the template for target i. The target template d_i^{pred} most similar to the observed data d^{obs} is selected as the most likely target.

There are a number of measures that compares the target templates with the observed data. Intuitively, these include measures of maximum correlation or minimum error. There are also several ways with which to define the minimum error. Riggs et al. (2001) outline the derivation of the minimum least squares from a generalized likelihood ratio test (GLRT) with Gaussian data statistics. The likelihood ratio test for two targets

$$\frac{p(d^{\text{obs}}|p_1)}{p(d^{\text{obs}}|p_2)} \underset{\text{target2}}{\overset{\text{target1}}{\lessgtr}} \frac{p(p_2)(C_{01}-C_{11})}{p(p_1)(C_{12}-C_{22})} \equiv \eta \tag{11}$$

where C_{ij} is the cost of classifying the target as p_i when the target is p_j, and $p(p_i)$ is the prior probability for the ith class. The GLRT is obtained by substituting the maximum likelihood estimate into Eq. (11). If we consider two targets with equal prior probability of producing the anomaly, and assuming that an incorrect classification produces the same cost, then $\eta=1$. By taking the logarithm of the resulting expression, our decision criterion is to simply select the target that has the smallest least squares error:

$$\begin{aligned} &\| V_d^{-1/2}(d^{\text{obs}}-F[r_1, \theta_1, \phi_1, p_1]) \|^2 \\ &\underset{\text{target2}}{\overset{\text{target1}}{\lessgtr}} \| V_d^{-1/2}(d^{\text{obs}}-F[r_2, \theta_2, \phi_2, p_2]) \|^2 \end{aligned} \tag{12}$$

where r_i is the position, and θ_i, and ϕ_i are the orientation angles that produces the best fits the observed data for the model p_i. For multiple candidate targets we simply choose the target with smallest least squares misfit.

Application of the above algorithm to survey data requires establishing two thresholds. First, a minimum

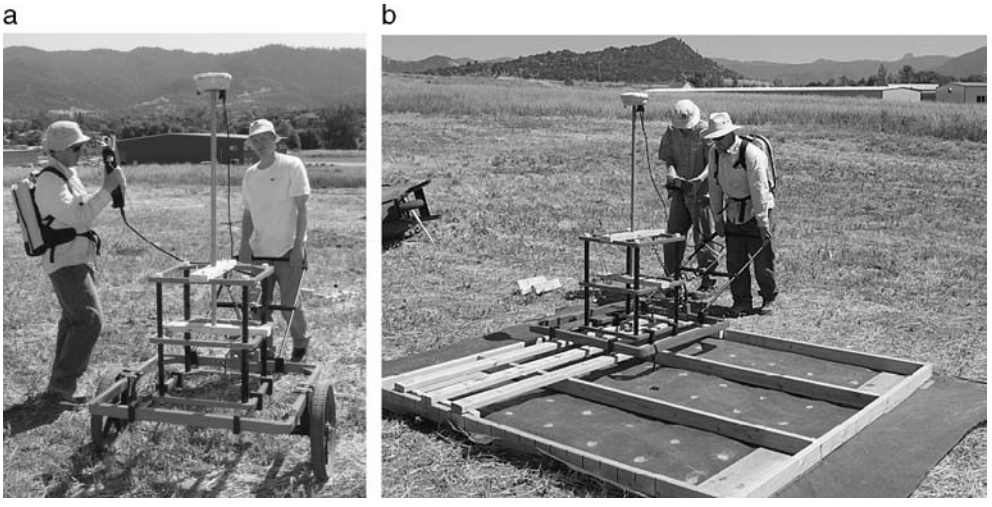


Fig. 2. (a) Dynamic data acquisition, (b) static data acquisition. Dynamic and static data acquisition modes using the Geonics EM63.

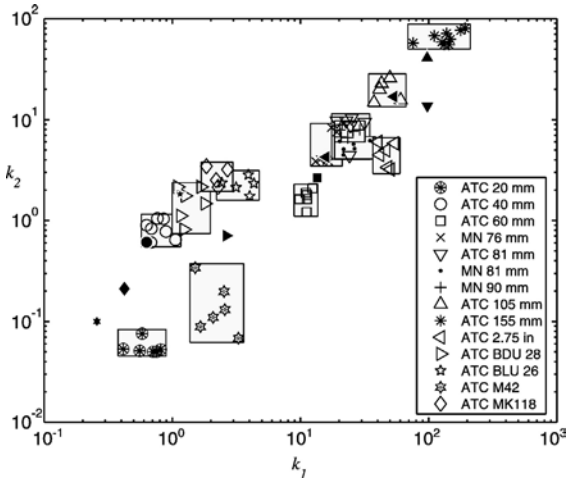


Fig. 3. Comparison of k_1 and k_2 parameters obtained by inverting ERDC test stand data. Solid symbols represent results from inverting dynamically collected blind test data.

level of data quality must be established, since our confidence in identifying the correct target decreases as the data quality worsens. For data sets acquired with the same survey parameters (such as station density) for the entire data set, the critical measure of data quality is the signal to noise ratio (S/N) ratio. A second threshold is a maximum misfit at which an anomaly can be labeled as a target within our library. Since the ability to distinguish differences between the observed data and the template data will depend on the quality of data, the minimum correlation threshold will also be dependent on the S/N ratio of the target. These thresholds can be established with training data or, if the survey noise can be accurately modeled, through simulations.

3. Results and analysis

3.1. Development of a target library from test stand data

Our UXO library consists 14 different targets: eleven items from the Aberdeen Test Center (ATC) Standardized UXO set and three ordnance from the Montana Army National Guard (MTARNG) (Table 1). These items represent a cross section of ordnance sizes from large to small and also include a few examples of submunitions. The ATC items were manufactured as inert UXO and have never been fired. The MTARNG items were fired and recovered from the Limestone Hills in Montana.

Geonics EM63 (Fig. 2) time domain data were collected over each item at the U.S. Army Engineer Research and Development Center (ERDC) test stand facility in Vicksburg, MS. Each item was measured at 3 orientations and 2 depths. The test stand makes it possible to collect geophysical data with highly repeatable positional information. It also enables us to collect data in an environment free of background geologic responses with the ordnance placed at an accurately known position and orientation relative to the geophysical sensor. The sensor is mounted on a robotic arm that is controlled by an external computer. Noise levels of the instrument were decreased by stacking multiple time domain decays at each sounding location.

The polarization tensors, represented by the set of decay parameters defined in Eq. (6), were determined by solving Eq. (9) for each set of data. Model constraints restricting the depth to within 10 cm of the true depth and orientation to within 5° of the true orientation were

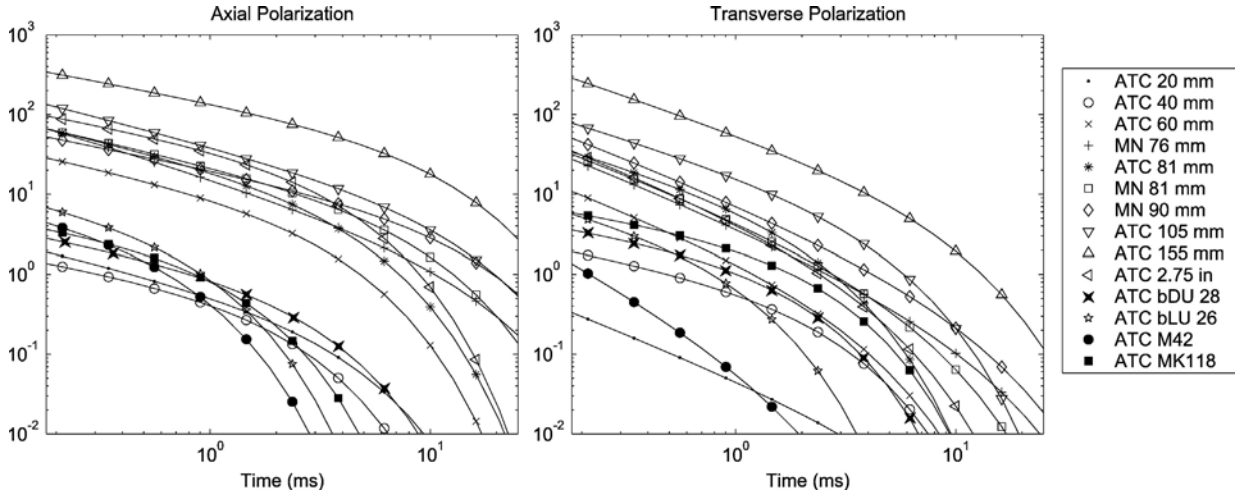


Fig. 4. Axial ($\partial L_1(t)/\partial t$) and transverse ($\partial L_2(t)/\partial t$) polarization curves for targets within our library. The units for the polarization curves are 1/s (i.e. s^{-1}).

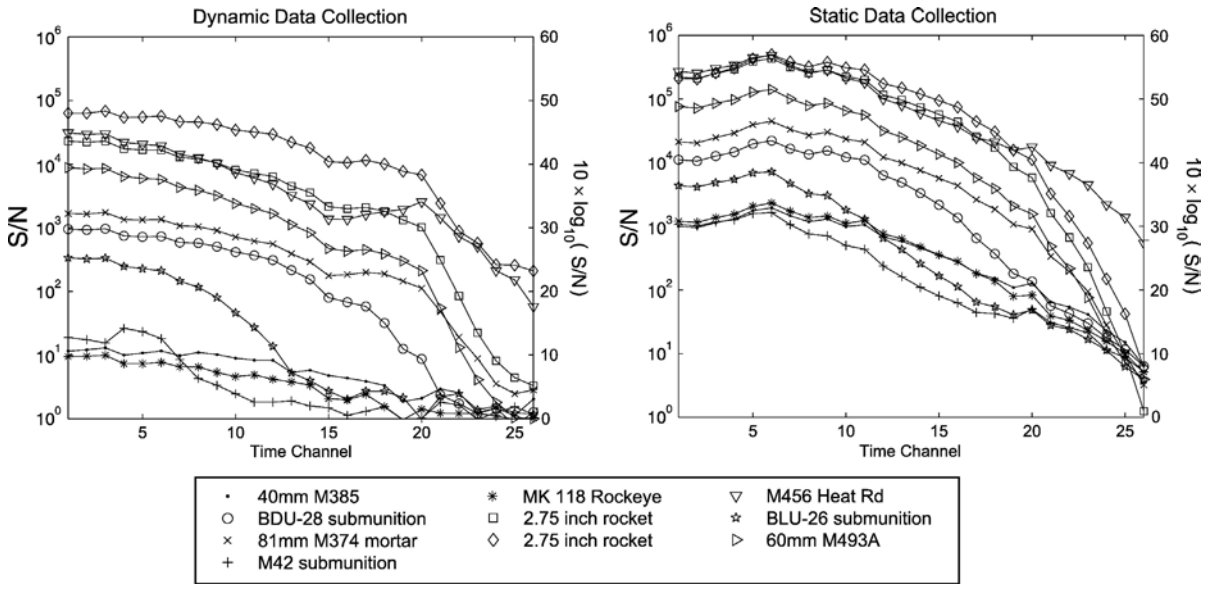


Fig. 5. Comparison of signal to noise ratio for data anomalies acquired statically and dynamically. The ten targets represent the targets in the blind test.

implemented when inverting for the decay parameters. Fig. 3 shows how the different targets separate within the k_1, k_2 of Eq. (6) feature space. Each target is well grouped in this space, albeit with some overlap. A rectangular box is drawn around each cluster. If the dipole model exactly described the response of each UXO, and if the data could constrain each inversion parameter, then each cluster would collapse to a single point in parameter space. We

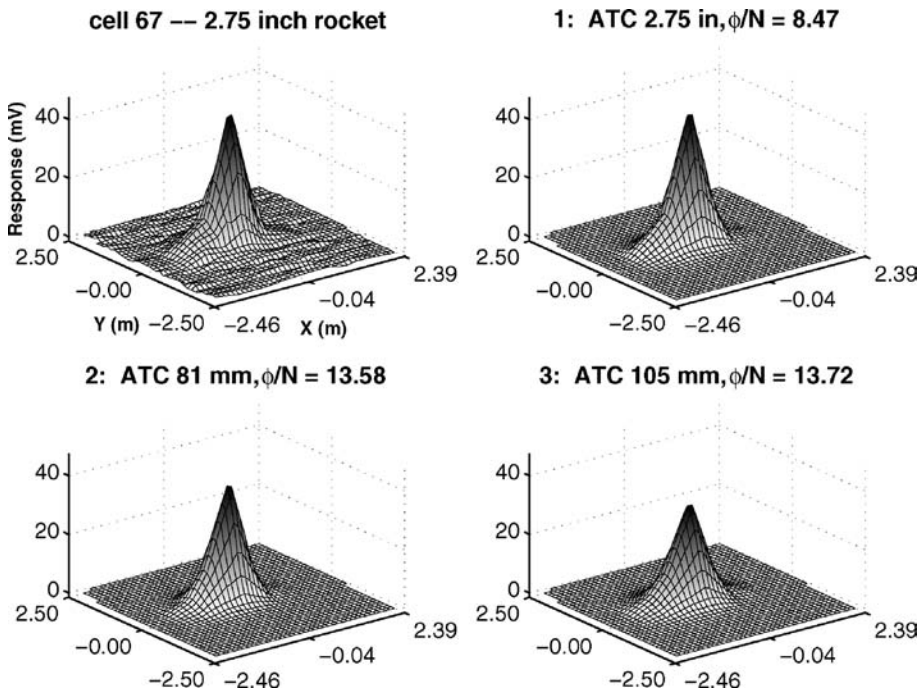


Fig. 6. Application of the library method to dynamically collected data measured over an ATC M230 2.75 in. rocket. The upper left panel contains the fifteenth time channel of observed data. The remaining panels represent the three most likely targets, ranked according to the normalized misfit ϕ/N.

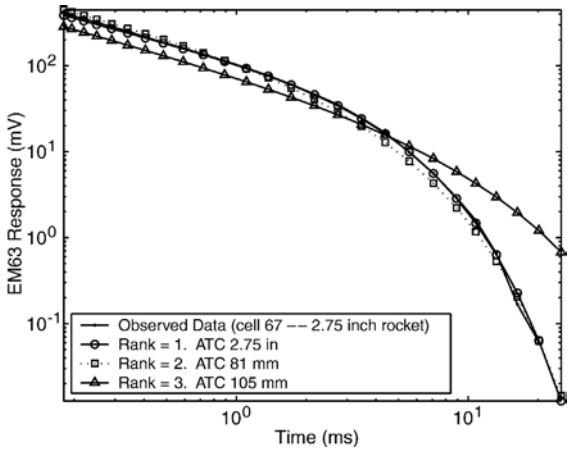


Fig. 7. Application of the library method to dynamically collected data measured over an ATC M230 2.75 in. rocket. The best fit soundings observed at a point directly over the rocket are plotted.

reduce the number of polarization tensors in our library to a single polarization by using the median value of each decay parameter. Fig. 4 plots the representative polarizations $\partial L_1(t)/\partial t$ and $\partial L_2(t)/\partial t$ for each target within the library.

3.2. Application of the library method to data collected at the Sky Research Ashland Test Plot Data

The library method was tested using data collected at the Sky Research UXO test plot in Ashland, Oregon. The test plot was seeded with a set of ordnance that included items from the ATC standardized test set, items from the MTARNG, as well as fragments of UXO. Multi-target and clutter scenarios are simulated within the test plot. The blind test, consisting of identifying the target present for ten anomalies within the test plot, was used to demonstrate the identification potential of the library procedure. This test represents the simplest identification problem for the library method since (1) each target was a member of the ordnance library and (2) each target anomaly was isolated (i.e. no overlapping signals due to nearby metal objects).

The library method was tested using dynamic and static collected data. Dynamic data collection describes a typical detection survey data acquisition where an area is covered by a series of data transects (Fig. 2(a)). The Geonics EM63 data were obtained with 0.5 m line spacing. A differential GPS was used for recording positioning. The sensor cart was not equipped with an orientation sensor to detect sensor tilting due to terrain. Therefore, we assumed that the transmitter loop was horizontal and at a height of 40 cm above the ground. A high pass filter was used to remove the effects of instrument drift and a background geologic signal.

In order to minimize Eq. (10), an estimate of the data covariance matrix V_d is required. For our data

Table 2
Blind test results when inverting dynamically acquired data

Actual target	Estimated target	Target list rank	Normalized misfit (ϕ/N)	Total S/N
ATC 40 mm M385	ATC MK118 Rockeye	3	0.8	241.0
ATC BDU-28 submunition	ATC MK118 Rockeye	2	2.7	3007.1
ATC 81 mm M374	ATC 81 mm M374	1	6.1	13,046.7
ATC M42 submunition	ATC M42 submunition	1	0.7	203.9
ATC MK118 Rockeye	ATC MK118 Rockeye	1	0.6	243.1
ATC M230 2.75″ Rockeye	ATC M230 2.75″ Rockeye	1	8.5	50,953.6
ATC M230 2.75″ Rockeye	ATC M230 2.75″ Rockeye	1	18.4	98,099.4
ATC 105 mm M456 heat rd	ATC 105 mm M456 heat rd	1	8.9	69,888.7
ATC BLU-26 submunition	ATC BLU-26 submunition	1	1.2	2011.4
ATC 60 mm M49A3	ATC 60 mm M49A3	1	4.1	14,548.1

Table 3
Blind test results when inverting static data

Actual target	Estimated target	Target list rank	Normalized misfit (ϕ/N)	Total S/N
ATC 40 mm M385	ATC 40 mm M385	1	1.5	9596.3
ATC BDU-28 submunition	ATC BDU-28 submunition	1	1.1	100,591.2
ATC 81 mm M374	ATC 81 mm M374	1	3.1	201,625.7
ATC M42 submunition	ATC M42 submunition	1	0.9	6931.8
ATC MK118 Rockeye	ATC BDU-28 submunition	4	1.1	11010.5
ATC M230 2.75″ Rockeye	ATC M230 2.75″ Rockeye	1	3.6	1,972,452.7
ATC M230 2.75″ Rockeye	ATC M230 2.75″ Rockeye	1	2.3	2,382,358.6
ATC 105 mm M456 heat rd	ATC 105 mm M456 heat rd	1	4.6	2,135,632.3
ATC BLU-26 submunition	ATC BLU-26 submunition	1	1.0	27,950.4
ATC 60 mm M49A3	ATC 60 mm M49A3	1	1.2	619,430.8

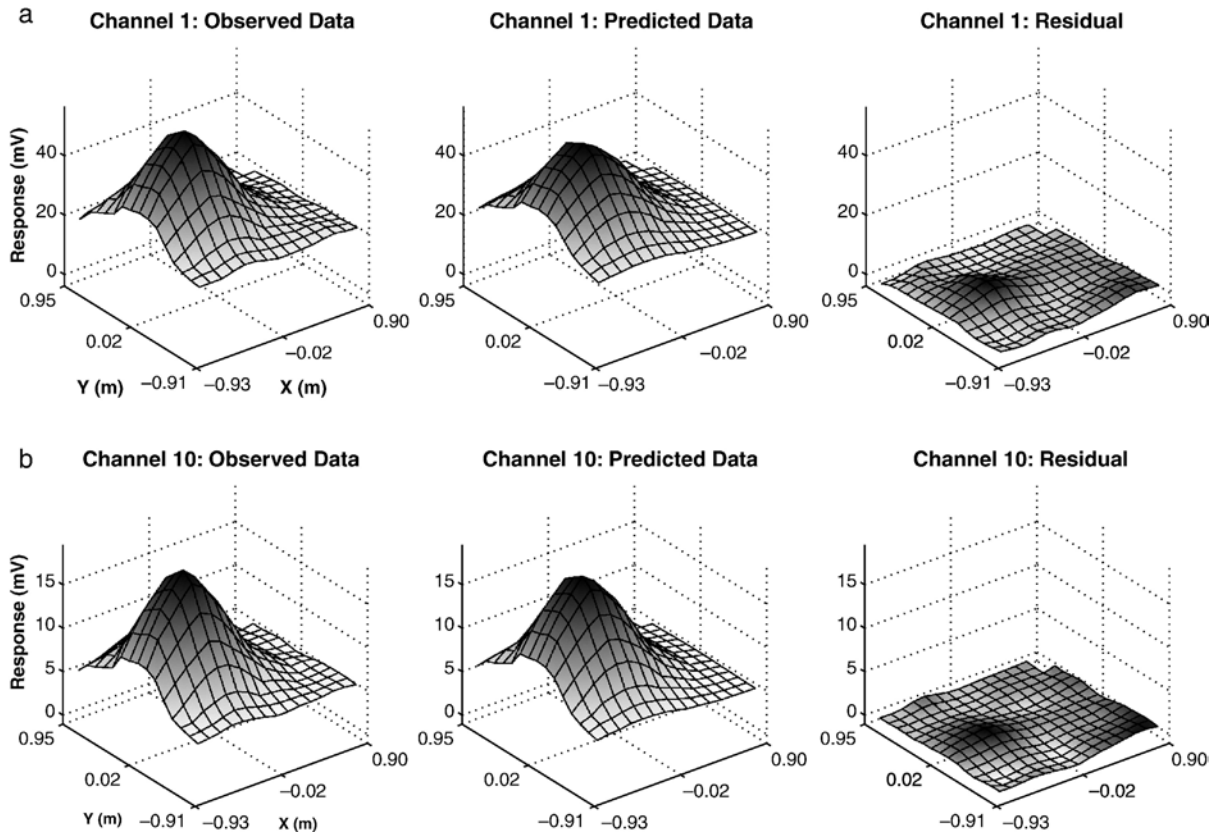


Fig. 8. (a) Channel 1, (b) channel 10. Data misfit when applying the library method to data statically collected over an ATC MK118. Possible reasons for the incorrect classification by the algorithm include incomplete spatial coverage of the anomaly and a large background geologic response.

inversion we assume that the data errors are uncorrelated, and that the diagonal components of the covariance matrix are defined as $[V_d^{1/2}]_{ii}=5\%\times d_i^{\mathrm{obs}}+\sigma_i$, where σ^i is the standard deviation of the noise. The noise analysis in Walker et al. (2007-this issue) is used for estimating σ_i. A standard deviation σ_i is defined for each time channel of data. Fig. 5 plots the S/N for each time channel of the ten anomalies in the blind test. For each anomaly, only time channels with a S/N greater than 5 were inverted. Data having amplitude less than twice the standard deviation of the noise were not included in the inversion.

The least squares solution was computed for each target in the library, and then the targets were ranked by their least squares misfit to the observed data. Figs. 6 and 7 demonstrate the results when applying this technique to data from an ATC M230 2.75 in. rocket. Fig. 6 plots the fifteenth time channel of data of the observed data and the predicted data from the three targets that best fit the data. The quality of fit is quantified by the least squares misfit divided by the number of data (ϕ/N). Fig. 7 shows the quality of fit of a TEM sounding measured directly above the target.

Results from applying the library technique to the dynamically collected data are summarized in Table 2. A list of the library targets, sorted by each target's ability to fit the data, is formed for each anomaly. The column labeled "Target Rank" indicates where the actual target was ranked by the algorithm. The column "Total S/N" is the sum of the signal to noise ratios calculated at each of the 26 time channels. The algorithm correctly identified eight of ten targets. The algorithm incorrectly classified the 40 mm as a MK118 Rockeye. This likely results because the anomaly from the 40 mm has a low S/N (see Fig. 5). The algorithm incorrectly classified BDU28 the anomaly as an MK118 Rockeye, while ranking the BDU28 as the second most likely target. Incorrect classification of the BDU28 may be due to the BDU28 and MK118 polarization tensors being too similar (Fig. 4), relative to the data's S/N, for the algorithm to make a correct identification. Higher quality data (i.e. data collected with improved positioning information and

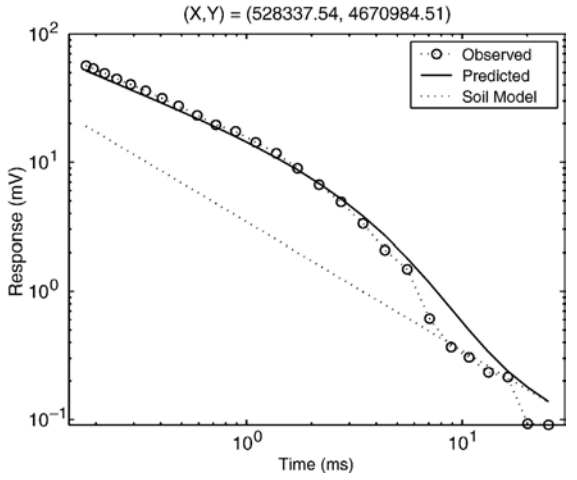


Fig. 9. Data misfit for a sounding taken directly over an ATC MK118. The estimated soil noise is of approximately the same order as the data, possibly causing the difficulty in correctly identifying the target.

lower S/N) is required to improve the performance of algorithm.

The dynamically acquired data were also inverted for the polarization tensor for comparison to the template matching technique. Fig. 3 compares the recovered k values (plotted with solid symbols), with the k parameter clusters derived from the ERDC test stand data. If we define identification according to the cluster closest to the recovered parameter, then the inversion would have correctly identified only three of the ten targets. Parametric inversion on these dynamically collected data is less successful than using the template approach. This is likely due to the noise levels of the data and the inaccuracies with which the position and orientation of the sensor was recorded.

The statically collected data represent a "cued interrogation" style of data acquisition. Static data were collected by placing a Geonics EM63 sensor without wheels on a portable test stand positioned over the target (Fig. 2(b)). The test stand was used to increase positioning accuracy and to reduce instrument noise by stacking multiple TEM soundings. Data were collected over a 1.8 m square area with measurements on a uniform grid with 30 cm station spacing. When placed on the stand, the transmitter coil of the EM63 was located 15 cm from the ground. The S/N of the data is improved by placing the sensor on a stable platform, close to the ground. Unfortunately, the close proximity of the transmitter coil to the ground introduces a significant soil response. Since the data were collected over a 1.8 m square area, a high pass filter could not be used to remove the background response. Therefore when solving for the least squares misfit (Eq. (12)) of each library target, a background soil model was included:

$$\text{minimize } \phi(m) = \frac{1}{2}\left|\left| V_d^{-1/2}\left[d^{\text{obs}} - \left(F[m] + \frac{A}{t}\right)\right]\right|\right|^2 \quad (13)$$

where $F[m]$ represents a dipole forward model, and the soil model is represented by A/t. This form of the soil

Table 4
Blind test results when inverting static data

Cell	Actual target	Rank	ϕ/N	Total S/N
56A	ATC 20 mm	7	1.1	176.7
56B	ATC 20 mm	1	2.4	2423.7
56C	ATC 20 mm	3	0.8	241.0
57A	ATC BDU 28	2	0.8	491.3
57B	ATC BDU 28	2	2.7	3007.1
57C	ATC BDU 28	4	2.2	2124.3
60	ATC 81 mm	1	6.1	13,046.7
61	ATC 81 mm	2	1.1	2433.1
62	ATC 81 mm	1	7.2	57,351.1
63	ATC 2.75 in.	1	4.1	23,445.1
64A	ATC 40 mm	3	0.8	533.6
64B	ATC 40 mm	2	1.4	939.5
64C	ATC M42	1	0.7	203.9
64D	ATC M42	1	1.4	768.7
65A	ATC MK118	1	0.6	243.1
65B	ATC MK118	3	0.6	503.3
65C	ATC MK118	1	1.4	4158.5
65D	ATC 60 mm	1	1.8	4602.7
67	ATC 2.75 in.	1	8.5	50,953.6
68	ATC 2.75 in.	1	18.4	98,099.4
69	ATC 105 mm	2	3.3	1395.2
70	ATC 105 mm	2	4.2	10,556.9
71	ATC 105 mm	1	8.9	69,888.7
72A	ATC M42	1	2.0	3022.0
72B	ATC BLU 26	1	1.2	2011.4
72C	ATC BLU 26	1	4.3	3839.7
72D	ATC BLU 26	1	2.3	2120.3
73A	ATC 60 mm	1	8.1	63,828.2
73B	ATC 60 mm	1	4.1	14,548.1
75	ATC 155 mm	1	6.5	17,542.9
76	ATC 155 mm	1	8.2	74,554.2
77	ATC 155 mm	1	16.0	347,888.0
78	MN 76 mm	3	2.7	3073.5
79	MN 76 mm	1	1.9	15,164.6
80	MN 76 mm	1	5.6	50,001.3
81	MN 81 mm	1	8.5	3269.2
82	MN 81 mm	1	8.2	44,246.4
83	MN 81 mm	1	4.5	32,537.6
84	MN 90 mm	1	3.7	7038.2
86	MN 90 mm	4	4.9	64,553.1
87	MN 90 mm	1	6.9	50,964.7

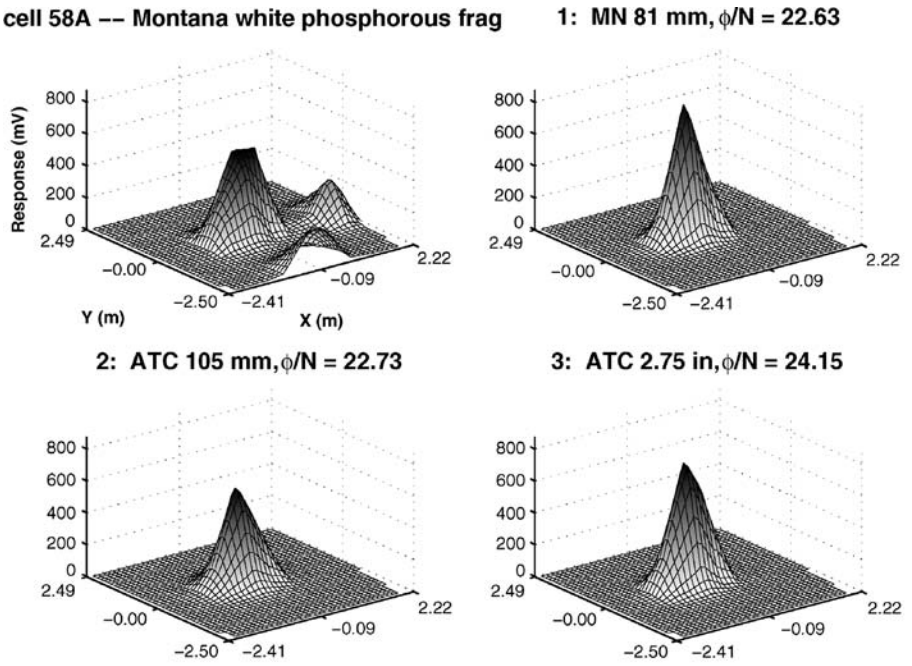


Fig. 10. Fitting results when applying the library matching to a metal scrap not included in the library. The first time channel of data is presented. The normalized misfit is higher than when fitting targets within the library.

model is representative of the response of a step-off time domain sensor to viscous remnant magnetized ground (Billings et al., 2003). Therefore, for each target in the library we solve for three location parameters, two orientation angles, and an amplitude of the background soil response. Similar to the dynamic case, data less than twice the standard deviation of the noise were not included in the inversion.

Results from applying the library technique to the statically collected data are summarized in Table 3. The algorithm correctly identified nine of the ten targets. The only misclassified anomaly was from a MK118 Rockeye. The algorithm classified the target as BDU28 submunition, while determining the MK118 Rockeye to be the fourth most likely library target. The data fit for this case is good as is demonstrated by Fig. 8 and the low normalized misfit (Table 3). The incorrect identification of the MK118 Rockeye may be related to a tradeoff between the parameter modeling the relatively large background soil signal in the data (approximately 20 mV in the first time channel) and the polarization tensor (Fig. 9). In addition, the anomaly was only partially sampled due to the test stand not being centered on the target; therefore less data were available to constrain the result.

Following the blind test, the library procedure was further tested by processing the remaining anomalies from the dynamically acquired test plot. The remaining anomalies included single isolated targets both belonging to, and not belonging to, our library, and target anomalies that were obscured by responses from nearby sources. Table 4 summarizes the results of applying the method to the single, isolated test plot targets that are also members of the library. Of these 41 anomalies, 28 were correctly identified, 6 of the anomalies had the correct target ranked second, and 4 of the anomalies had

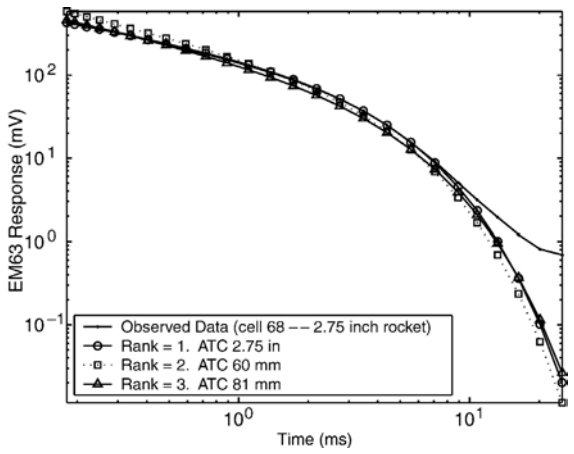


Fig. 11. Application of the library method to cell 68 containing a 2.75 in. rocket. Even though the anomaly was correctly identified, the feature in the data at late time result in an atypically large misfit.

the correct target ranked third. Misclassified targets are generally due to low signal to noise ratios.

In order for the library method to be an attractive technique for processing TEM data, we must be able to identify anomalies due to targets not included in our target library. Fig. 10 has an example of fitting non-UXO scrap. The metallic scrap is a fragment from a 105 mm white phosphorous round, and is not included in our library of targets. The first time channel of the data is plotted. The secondary anomaly in the data, to the right of the main peak, was assumed to be from an adjacent target and, therefore, not included in the data fitting. The normalized misfit is larger than most of the fits in Table 4, indicating that none of the templates from our library fits the data well. This suggests that a threshold on the normalized misfit could be established for classifying the target as a member of our library. However, the misfit is sensitive to non-dipolar features in the noise. For example, cell 68 containing a 2.75 in. rocket, has nearly the same normalized misfit due to signal at late time not being accurately modeled (Fig. 11). Unfortunately, there are not enough targets in this example to establish a reliable threshold. Application of this method to real world UXO applications should be preceded with careful noise analysis of the data and Monte Carlo studies for establishing a useful threshold for classification.

4. Conclusion

In this paper we applied a simple library based technique for processing time domain electromagnetic data. This technique avoids direct inversion for polarization tensor parameters, making it more feasible for cases where sensor data quality might not be sufficient to support confident estimation of model parameters. The performance of the algorithm is limited by the data quality and the differences of polarization tensors for different targets. Targets with similar polarization tensors would be indistinguishable to this algorithm.

This library based technique can be applied to any type of electromagnetic sensor. Indeed, the performance of the technique would improve if the data were able to sense each of the three stages of the time decay, since the magnetic crossover time, the power law decay, and the fundamental time constant each contain information on the shape and material properties of the target. If the data were sensitive to non-dipole features of the response, non-dipole type models could be implemented. If these models had parameters that reflect the target shape features that produce higher order poles, there would likely be a greater separation within parameter space (compared to dipole polarization models) and better performance of the library technique.

Geonics EM63 data acquired in dynamic and static modes were used to test this technique. A blind test demonstrated an ability to accurately identify single targets when the target was a member of the UXO library. Misidentification of single targets was due to either low signal to noise ratios of data anomalies or because different items had similar polarization tensors. In cases where there was a significant background signal due to magnetic ground, the library technique showed improved performance by simultaneously solving for the best fit background soil model with the dipole parameters.

The work in this paper represent preliminary tests of the library method. Before this method can be implemented in a practical setting, tests are required to determine robustness to noise and other data quality factors, such as positional accuracy and spatial data coverage. Work is required to determine an optimal measure for determining whether we can classify an anomaly as coming from a target that is not a member of the library. A series of Monte Carlo style simulations should be carried out in order to investigate these questions.

Acknowledgments

Funding for this work was provided, in part, by the U. S. Army Research and Development Center project W912HZ-04-C-0039. Assistance at the ERDC test stand was provided by USACE-ERDC personnel Cliff Morgan, Morris Fields, and Charles Hahn. Laurens Beran and Mark Fallat also helped collect ERDC test stand data. Jon Jacobson and Kevin Kingdon helped collect the cued interrogation data at the Sky Research UXO Test Site.

References

Bell, T., 2005. Geo-location requirements for uxo discrimination. SERDP and ESTCP Geolocation Workshop.

Bell, T., Barrow, B., Miller, J., 2001a. Subsurface discrimination using electromagnetic induction sensors. IEEE Transactions Geoscience and Remote Sensing 39, 1286–1293.

Bell, T., Barrow, B., Miller, J., Keiswetter, D., 2001b. Time and frequency domain electromagnetic induction signatures of unexploded ordnance. Subsurface Sensing Technologies and Applications 2 (3), 153–175.

Beran, L., 2005. Classification of unexploded ordnance. Master's thesis, University of British Columbia.

Billings, S.D., 2004. Discrimination and classification of buried unexploded ordnance using magnetometry. IEEE Transactions Geoscience and Remote Sensing 42, 1241–1251.

Billings, S., Pasion, L., Oldenburg, D., Foley, J., 2003. The influence of magnetic viscosity on electromagnetic sensors. Proceedings of EUDEM-SCOT2, International Conference on Requirements and

Technologies for the Detection, Removal and Neutralization of Landmines and UXO.

Carin, L., Yu, H., Dalichaouch, Y., Perry, A., Czipott, R., Baum, V., 2001. On the wideband emi response of a rotationally symmetric permeable and conducting target. IEEE Transactions on Geoscience and Remote Sensing 39 (6), 1206–1213 June.

Casey, K.F., Baertlein, B.A., 1999. An Overview of Electromagnetic Methods In Subsurface Detection. Taylor and Francis, Ch. The Magnetic Polarizability Dyadic and Point Symmetry, pp. 9–46.

Collins, L., Zhang, Y., Li, J., Wang, H., Carin, L., Hart, S., Rose-Pehrsson, S., Nelson, H., McDonald, J., 2001. A comparison of the performance of statistical and fuzzy algorithms for unexploded ordnance detection. IEEE Transactions on Fuzzy Systems 9 (1), 17–30 February.

Grimm, R., 2003. Triaxial modeling and target classification of multichannel, multicomponent EM data for uxo discrimination. Journal of Engineering and Environmental Geophysics 8 (4), 239–250.

Grimm, R.E., Blohm, M.W., Lavely, E.M., 1997. Uxo characterization using multicomponent, multichannel time-domain electromagnetic induction. Proceedings of UXO Forum '97.

Istratov, A.A., Vyvenko, O.F., 1999. Exponential analysis in physical phenomena. Review of Scientific Instruments 70 (2), 1233–1257.

Kaufman, A.A., 1994. Geophysical Field Theory and Method. Academic Press.

Norton, S., Won, I., Cespedes, E., 2001. Spectral identification of buried unexploded ordnance from low-frequency electromagnetic data. Subsurface Sensing Technologies and Applications 2 (3), 177–189.

Pasion, L.R., 1999. Detecting unexploded ordnance with time domain electromagnetic induction. Master's thesis, University of British Columbia.

Pasion, L.R., Oldenburg, D.W., 2001. A discrimination algorithm for uxo using time domain electromagnetics. Journal of Engineering and Environmental Geophysics 6 (2), 91–102.

Pasion, L., Billings, S., Oldenburg, D., 2003. Joint and cooperative inversion of magnetic and time domain electromagnetic data for the characterization of uxo. Proceedings from SAGEEP 03.

Pasion, L.R., Billings, S.D., Oldenburg, D.W., 2004. Guidelines on data quality requirements for advanced discrimination of uxo. Tech. rep., U.S. Army Research and Development Center, Vicksburg, MS, project Number DACA42-03-P-0238.

Riggs, L., Mooney, J., Lawrence, D., 2001. Identification of metallic mine-like objects using low frequency magnetic fields. IEEE Transactions on Geoscience and Remote Sensing 39 (1).

Shamatava, I., Shubitidze, F., Chen, C., Youn, H., O'Neill, K., Sun, K., 2004. Potential benefits of combining emi and gpr for enhanced uxo discrimination at highly contaminated sites. Proceedings of SPIE Detection and Remediation Technologies for Mines and Minelike Targets IX, vol. 5415 (September).

Smith, J., Morrison, H.F., Becker, A., 2004. Parametric forms and the inductive response of a permeable conducting sphere. Journal of Environmental and Engineering Geophysics 9, 213–216.

Snyder, D.D., MacInnes, S., Urquhart, S., Zonge, K.L., 1999. Possibilities for uxo classification using characteristic modes of the broad-band electromagnetic induction response. Proceedings of A New Technology Applications Conference on the Science and Technology of Unexploded Ordnance Removal and Site Remediation.

Tantum, S.L., Collins, L.M., 2001. A comparison of algorithms for subsurface target detection and identification using time-domain electromagnetic induction data. IEEE Transactions on Geoscience and Remote Sensing 39 (6), 1299–1306 June.

Walker, S.E., Pasion, L.R., Oldenburg, D.W., Billings, S.D., 2007. Investigating the effect of data quality on time domain electromagnetic discrimination. Journal of Applied Geophysics 61, 254–278 (this issue). doi:10.1016/j.jappgeo.2006.05.005.

Weichman, P.B., 2004. Surface modes and multipower-law structure in the early-time electromagnetic response of magnetic targets. Physical Review Letters 93 (2) Jul.

Zhang, Y., Collins, L., Yu, H., Baum, C.E., Carin, L., 2003. Sensing of unexploded ordnance with magnetometer and induction data: theory and signal processing. IEEE Transactions on Geoscience and Remote Sensing 41 (5), 1005–1015 May.